HHS Public Access

Author manuscript

Acta Biomater. Author manuscript; available in PMC 2020 August 01.

Published in final edited form as:

Acta Biomater. 2019 August ; 94: 183–194. doi:10.1016/j.actbio.2019.05.063.

Differential outcomes of venous and arterial tissue engineered vascular grafts highlight the importance of coupling long-term implantation studies with computational modeling

Cameron A. Best[1,2,*,†], **Jason M. Szafron**[3,*], **Kevin A. Rocco**[5,*], **Jacob Zbinden**[1,6], **Ethan W. Dean**[7], **Mark W. Maxfield**[8], **Hirotsugu Kurobe**[9], **Shuhei Tara**[10], **Paul S. Bagi**[11], **Brooks V. Udelsman**[12], **Ramak Khosravi**[3,4], **Tai Yi**[1], **Toshiharu Shinoka**[1,13], **Jay D. Humphrey**[3,4], **Christopher K. Breuer**[1,14]

[1.]Center for Regenerative Medicine, Tissue Engineering Program, The Research Institute at Nationwide Children's Hospital, Columbus OH

[2.]Biomedical Sciences Graduate Program, The Ohio State University College of Medicine, Columbus OH

[3.]Department of Biomedical Engineering, Yale University, New Haven CT

[4.]Vascular Biology and Therapeutics Program, Yale University School of Medicine, New Haven CT

[5.]Biorez, Inc., New Haven CT

[6.]Biomedical Engineering Graduate Program, The Ohio State University College of Engineering, Columbus OH

[7.]Department of Orthopaedic Surgery, University of Florida, Gainesville, FL

[8.]Department of Thoracic Surgery, University of Massachusetts Memorial Medical Center, Worcester MA

[9.]Department of Cardiovascular Surgery, Institute of Biomedical Sciences, Tokushima University Graduate School, Tokushima, Japan

[10.]Department of Cardiovascular Medicine, Nippon Medical School, Tokyo, Japan

[11.]Department of Orthopaedic Surgery, Yale-New Haven Hospital, New Haven CT

[12.]Department of Surgery, Massachusetts General Hospital, Boston MA

[13.]Department of Cardiac Surgery, Nationwide Children's Hospital, Columbus OH

[†]Corresponding/Reprint Author:.Cameron Best, Tissue Engineering Program, Center for Regenerative Medicine, The Research Institute at Nationwide Children's Hospital, 575 Children's Crossroad – WB4154, Columbus, OH 43215, Phone: 614.355.5803, Cameron.Best@nationwidechildrens.org.

[*]Cameron Best, Jason Szafron, and Kevin Rocco contributed equally

Data Availability

The authors confirm that the raw/processed data supporting the findings of this study are available from the corresponding author upon reasonable request.

[14]Department of Surgery, Nationwide Children's Hospital, Columbus OH

Abstract

Electrospinning is commonly used to generate polymeric scaffolds for tissue engineering. Using this approach, we developed a small-diameter tissue engineered vascular graft (TEVG) composed of poly-ε-caprolactone-co-L-lactic acid (PCLA) fibers and longitudinally assessed its performance within both the venous and arterial circulations of immunodeficient (SCID/bg) mice. Based on *in vitro* analysis demonstrating complete loss of graft strength by 12 weeks, we evaluated neovessel formation *in vivo* over 6-, 12- and 24-week periods. Mid-term observations indicated physiologic graft function, characterized by 100% patency and luminal matching with adjoining native vessel in both the venous and arterial circulations. An active and robust remodeling process was characterized by a confluent endothelial cell monolayer, macrophage infiltrate, and extracellular matrix deposition and remodeling. Long-term follow-up of venous TEVGs at 24 weeks revealed viable neovessel formation beyond graft degradation when implanted in this high flow, low-pressure environment. Arterial TEVGs experienced catastrophic graft failure due to aneurysmal dilatation and rupture after 14 weeks. Scaffold parameters such as porosity, fiber diameter, and degradation rate informed a previously described computational model of vascular growth and remodeling, and simulations predicted the gross differential performance of the venous and arterial TEVGs over the 24-week time course. Taken together, these results highlight the requirement for *in vivo* implantation studies to extend past the critical time period of polymer degradation, the importance of differential neotissue deposition relative to the mechanical (pressure) environment, and further support the utility of predictive modeling in the design, use, and evaluation of TEVGs *in vivo*.

Graphical abstract

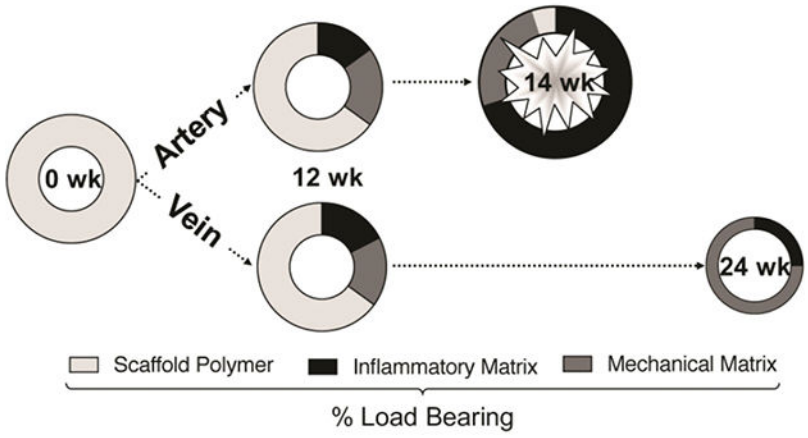

Keywords

electrospinning; tissue-engineered vascular graft; biodegradable scaffold; neovessel; predictive modelling

1. Introduction

Autologous vascular grafts are commonly utilized for vascular bypass procedures and demonstrate low rates of thrombosis and restenosis; however, they are limited in supply and quality, and add to procedure time and complexity [1,2]. In contrast, synthetic vascular grafts fabricated from materials such as Gore-Tex® and Dacron® are readily available, but do not assimilate *in vivo* and are susceptible to complications arising from infection/rejection, neointimal hyperplasia/stenosis, thrombosis, and calcification [2–4]. In small-diameter applications (<6mm), such as coronary bypass procedures, synthetic grafts are plagued by poor performance and their usage is contraindicated [5]. Thus, there exists a pressing clinical need for a readily available, durable, functional vascular conduit for small diameter vascular bypass applications.

Tissue engineering offers the potential to construct such an ideal vascular graft: one that is easily implanted, biomimetic, resists infection, rejection, thrombosis, stenosis, aneurysm, and ultimately transforms into a living vessel capable of growth, remodeling, and repair [2,6,7]. So called tissue-engineered vascular grafts (TEVGs) can be created from a biocompatible and bioresorbable polymeric scaffold whose structural and mechanical properties guide cellular infiltration and extracellular matrix (ECM) formation *in vivo* as the scaffold degrades, ultimately resulting in a scaffold-free neovessel that is similar in structure and function to native tissue. Our group has demonstrated successful clinical application of this approach in a high-flow, low pressure configuration for congenital heart repair with favorable long-term outcomes [8]. The growth potential of TEVGs is especially desirable for pediatric patients, who eventually outgrow traditional synthetic grafts and require additional “upsizing” operations, which carry significant risk of morbidity and mortality [7,9].

A variety of methodologies have been developed in pursuit of the ideal TEVG and are discussed in detail elsewhere [10–14]. Interestingly, few, if any, strategies have received as much attention as those using electrospinning [15]. Control over process parameters such as the polymer type(s), solution flow rate, solution concentration, and applied voltage permits careful engineering of scaffold properties such as fiber diameter, pore size (3-D void space between fibers), mechanical strength, compliance, and scaffold degradation rate [16–19]. Microfiber textiles, those having average fiber diameters of less than 1 μm, offer unique benefits for cellular interactions including attachment, proliferation, and differentiation, as a result of similarity in size and orientation to extracellular matrix components such as collagen fibrils [20–23]. Electrospun vascular conduits are fabricated by collecting the fibers around a grounded, rotating mandrel, and when implanted, improve cellular infiltration and endothelialization rates over standard synthetic grafts [24]. Despite these potential advantages, there has yet to be a report of an electrospun vascular conduit yielding a viable neovessel past complete polymer degradation. A literature review of electrospun TEVGs identified 28 published reports of *in vivo* implantation in a variety of animal models through 2014 [25]. An updated supplementary review highlights a striking observation: there has yet to be a report of an electrospun TEVG fully degrading and remodeling into a functional neovessel *in vivo* (Table 1).

To help understand the evolving biomechanical and morphologic characteristics of such TEVGs, computational growth and remodeling (G&R) models have been developed that capture salient aspects of the experimental data using numerical simulations [26,27]. These models have shown utility in predicting long-term graft behavior [28], and parametric studies have examined the effects of varying scaffold parameters on TEVG performance [29]. A computational model able to accurately predict TEVG G&R would favor an approach in which *in silico* studies could reduce the need for iterative *in vivo* experimentation during the initial stages of tissue engineering scaffold design. With this framework, simulated behavior of various scaffold iterations can be rapidly performed, thus allowing a more rational selection of candidate scaffolds to validate *in vivo*.

In the absence of adequate long-term studies on the performance of electrospun TEVGs *in vivo,* we sought to assess both *in vivo* and *in silico* the long-term performance of a rapidly degrading electrospun TEVG. The objectives of this study were twofold: 1) to design and evaluate *in vivo* an electrospun microfiber TEVG and assess safety and efficacy in high and low-pressure environments for a duration exceeding polymer degradation observed *in vitro* and 2) to test the predictive capacity of our computational G&R framework as applied to this novel scaffold over a 24-week time course in the arterial and venous circulations of the mouse. In this report, we demonstrate the importance of *in vivo* implantation studies extending beyond loss of scaffold integrity and extend the utility of our computational model in predicting TEVG behavior.

2. Materials and Methods

2.1 Scaffold Fabrication

Electrospinning process parameters, including solution concentration, voltage, flow rate, and distance to collector, were optimized to produce consistent, smooth fibers approaching 1 μm in diameter. Scaffolds were fabricated using a 6% (w/v) solution of a 50:50 co-polymer of poly (ε-caprolactone) and poly (ι-lactic acid) (PCLA, Gunze Corporation, Tokyo, Japan) dissolved in dichloromethane (Fisher Scientific, Pittsburgh, PA). The electrospinning apparatus consisted of a syringe pump (Harvard Apparatus, Holliston, MA), high-voltage power supply (Glassman High Voltage, High Bridge, NJ), and a rotating fiber-collection mandrel (Malin Company, Cleveland, OH). A positive voltage of 20 kilovolts was applied to an 18-gauge stainless steel blunted syringe tip (Popper & Sons, New Hyde Park, NY) through which copolymer solution was expelled at a controlled rate of 3.0 ml/hr. Extruded polymer fibers were collected around a revolving grounded mandrel, set 35.0 cm from the syringe tip, measuring 0.61 mm in diameter, and spinning at a frequency of 250 rpm. Resulting scaffolds were removed from the mandrel and cut to desired length (3.0 mm).

2.2 Scanning Electron Microscopy

Electrospun fiber formation and scaffold characteristics were evaluated using a FEI XL-30 scanning electron microscope (SEM, FEI, Hillsboro, OR). Average fiber diameter and average pore diameter were measured and calculated from representative SEM images using ImageJ software (n=300 images). Pore size measurements were further characterized using

both maximum and minimum Feret diameter using ImageJ software (National Institutes of Health, Bethesda, Maryland).

2.3 In vitro scaffold degradation

Scaffold degradation was characterized *in vitro* by incubating grafts in PBS at 37°C (without shaking) and evaluating changes in tensile strength, mass, and surface topography (n=6 per time point). The incubation solution was exchanged weekly, and the pH of the solution remained stable for the duration of the study. Ultimate tensile strength was serially assessed by vertically hanging a tensile load and increasing the load at a rate of 10g/min until failure. Mass loss was determined gravimetrically at each time point using an analytical balance (Mettler Toledo, Columbus, OH). Surface topography was imaged by SEM after sputter-coating with palladium.

2.4 In vivo study

The Institutional Animal Care and Use Committee at Yale University approved the use of animals and all procedures described in this study. Electrospun PCLA scaffolds were implanted as abdominal aortic interposition grafts (n=6) or inferior vena cava interposition grafts (n=6) in female C.B-17 severe combined immunodeficient-beige (SCID/bg) mice (Taconic, Rensselaer, NY), aged 16 weeks with body mass between 19 and 23 grams. Mice were anesthetized using an intraperitoneal injection of ketamine and xylazine (100μl/g) and opened with an abdominal midline incision. Abdominal organs were eviscerated, and a 3.0 mm portion of the infrarenal abdominal aorta (IAA) or inferior vena cava (IVC) was exposed under 5× magnification, clamped, and excised. 3.0mm long scaffolds (luminal diameter: 526.4±22.6μm and wall thickness: 234.8±20.3μm) were then implanted as interposition grafts using a running 10-0 nylon suture for the end-to-end anastomoses. The animals received routine postoperative care and were maintained without any anti-coagulation or anti-platelet therapy.

2.5 Serial monitoring of TEVG lumen diameter

TEVGs and the adjacent vessel were monitored postoperatively over 9 weeks using high-frequency doppler ultrasound (Vevo Visualsonics, Toronto, Canada). All imaging sessions were performed under anesthesia induced with 1.5% inhaled isoflurane. Mean luminal diameters of venous and arterial TEVGs were normalized to adjacent native vessel diameters measured using ImageJ software (n=3 measurements / vessel region of interest).

2.6 Histology and immunohistochemistry

Explanted grafts from each group were fixed in 10% (v/v) neutral buffered formalin, embedded in paraffin, and serially sectioned using previously described methods[52]. Histological staining included hematoxylin and eosin (H&E) and Masson's Trichrome (MT). Endothelial cells, smooth muscle cells, macrophages, and matrix metalloproteinase-2 (MMP-2) were identified by immunohistochemical staining using rabbit-anti human von Willebrand Factor (vWF, 1:1000, Dako, Carpinteria,CA), mouse-anti-human alpha smooth muscle actin (α-SMA, 1:1000, Dako), rat-anti-mouse F4/80 (1:1000, AbD Serotec, Oxford, UK), and rabbit-anti-human matrix metalloproteinase-2 (MMP-2, 1:200, Abeam,

Cambridge, UK), respectively. Antibody binding for vWF, α-SMA, F4/80, and MMP-2 was detected using biotinylated goat-anti-rabbit IgG (1:200, Vector Laboratories, Burlingame, CA), biotinylated goat-anti-mouse IgG (1:200, Vector), biotinylated goat-anti-rat IgG (1:200, Vector), and biotinylated goat-anti-rabbit IgG (1:200, Vector), respectively. This was followed by binding of streptavidin horseradish peroxidase (Vector) and chromogenic development with 3,3-diaminobenzidine (Vector). Sections were counterstained with hematoxylin (Gills Formula, Vector) to identify cell nuclei and cover slipped. Bright field photomicrographs were obtained at 20× magnification with a Zeiss Axio lmager.A2 microscope and associated Zeiss AxioCam MRc5 digital camera. Histologic and immunohistochemical stains were evaluated qualitatively.

2.7 Computational modeling

We used our constrained mixture model-based G&R framework [53], specialized for TEVGs [26], to predict the evolving geometries of the implanted grafts [27]. Individual, structurally significant constituents $\alpha = 1,\ldots, n$ are given rates of production and degradation, as well as material properties, that vary with time. Each constituent is constrained to deform with the graft as a whole, such that the constituent-specific deformation gradient at a current G&R time s for material produced at an intermediate G&R time τ is written as $\mathbf{F}^{\alpha}_{n(\tau)} = \mathbf{F}(s)\mathbf{F}^{-1}(\tau)\mathbf{G}^{\alpha}(\tau)$, where $\mathbf{F}$ is the deformation gradient for the bulk material and $\mathbf{G}^{\alpha}$ is the constituent deposition stretch. We use a simple rule of mixtures such that the stored energy of the bulk material is the sum of constituent stored energy densities with $W = \sum W^{\alpha}$, which allows a classical continuum formulation of the wall mechanics with Cauchy stress $\mathbf{t} = 2\det(\mathbf{F})\mathbf{F}\partial W/\partial \mathbf{C}\,\mathbf{F}^{T}$, where $\mathbf{C} = \mathbf{F}^{T}\mathbf{F}$ is the right Cauchy-Green tensor. G&R is assumed to yield a series of quasi-static states such that equilibrium is satisfied by $div\mathbf{t} = 0$. Constituent-specific stored energy density evolves as

$$\rho(s)W^{\alpha}(s) = \rho^{\alpha}(0)Q^{\alpha}(s)\widehat{W}^{\alpha}\left(\mathbf{F}^{\alpha}_{n(0)}(s)\right) + \int_0^s m^{\alpha}(\tau)q^{\alpha}(s,\tau)\widehat{W}^{\alpha}\left(\mathbf{F}^{\alpha}_{n(\tau)}(s)\right)d\tau,$$

where $\rho(s)$ is the overall graft density, $\rho^{\alpha}(0)$ is the initial apparent mass density of each constituent, $\widehat{W}^{\alpha}\left(\mathbf{F}^{\alpha}_{n(0)}(s)\right)$ is the stored energy density of the material produced at or before time 0, $m^{\alpha}(\tau)$ is the mass density production rate, $q^{\alpha}(s,\tau)$ is the survival fraction of material produced at time τ that remains at time s, and $\widehat{W}^{\alpha}\left(\mathbf{F}^{\alpha}_{n(\tau)}(s)\right)$ is the energy stored in the cohort of constituent α produced at time τ that remains at time s. Mechanical and immunological stimuli are both considered to have an effect on matrix and cellular properties with distinct behaviors prescribed for constituents mediated by either stimulus. Generally, production and degradation rates are higher for immune-mediated constituents, which also show elevated stiffness. Scaffold microstructure modulates the immune-mediated kinetics due to the reported effects of pore size and fiber diameter on infiltration and phenotype of cells [54,55]. The porosity of the scaffold can be calculated from statistical arguments using pore size and fiber diameter, which then characterizes scaffold mechanical behavior. Mechano-mediated kinetics are regulated by deviations from the homeostatic mechanical state [56], as cells are known to seek to maintain mechanobiological homeostasis [57].

The polymeric scaffold, denoted by $\alpha = p$, is present initially with no subsequent mass production, i.e. $m^p(\tau) = 0$. Degradation of PCLA is characterized by a sigmoidal degradation $Q^p(s) = (1 + \exp(-k^p\zeta^p)) / (1 + \exp(k^p(s - \zeta^p)))$ with k^p the polymer degradation rate and ζ^p a polymer degradation shape parameter. Polymer degradation is accelerated *in vivo*, hence we let $k^p = \gamma_D^i k_E^p$ and $\zeta^p = \zeta_E^p \Big/ \gamma_D^i$. A neo-Hookean form for the stored energy density of the polymer is $\widehat{W}^p(\mathbf{F}^p_{n(0)}(s)) = \mu^p(s)(\mathrm{tr}(\mathbf{C}^p_{n(0)}(s)) - 3)$ where the loss of mechanical integrity in the scaffold is captured by a varying shear modulus $\mu^p(s) = 0.03E_B^p(1 - \varepsilon^p(s))^2$ with E_B^p the Young's-like modulus of the bulk polymer and $\varepsilon^p(s)$ the evolving porosity of the scaffold.

The evolving biomechanical and geometric behavior of a porous TEVG implanted in the IVC of the SCID/bg mouse was previously captured with these G&R methods [27]. As the scaffold in this work is a different material and fabricated with different methods, the parameters describing the polymer microstructure and mechanical properties were adjusted to reflect data from the literature or matched to data collected experimentally (Table 2). For the venous circulation, hemodynamic parameters were the same as in previous works [26,27]. For the arterial circulation, hemodynamic parameters were varied to reflect luminal pressure and wall shear stress consistent with experimentally observed values [56].

2.8 Statistical methods

Data are reported and visualized as mean ± standard deviation unless indicated otherwise. No statistical hypothesis testing was performed as this was an exploratory observational study.

3. Results

3.1 Scaffold morphology

Electrospinning produced a non-woven scaffold with a fiber diameter of 882±226 nm and a 3-dimensional porosity as confirmed by SEM (Figure 1 A–E). Seamless conduits resulted from rotating the collection mandrel and the final conduits had a lumen diameter of 526.4±22.6μm and a wall thickness of 234.8±20.3 μm. Each conduit measured approximately 3.0 mm in length following trimming to meet appropriate surgical dimensions (Figure 1 F). The maximum and minimum Feret pore diameters were 6.33±0.21 μm and 3.34±0.12 μm, respectively (Figure 1 G).

3.2 In vitro scaffold degradation

Complete loss of tensile strength was observed by week 12, yet 71.45% of original scaffold mass remained after 21 weeks (Figure 2 A). Surface topography of the graft remained intact at 12 weeks (Figure 2 B), but degradation was evident at week 18 (Figure 2 C).

3.3 In vivo evaluation

The surgical handling characteristics of the graft were satisfactory with no observed transmural bleeding, thus eliminating the need for a clotting agent. There was also no indication of an acute thrombotic response in these SCID/bg mice. Serial ultrasound

confirmed 100% vessel patency in both groups. After 10 weeks, the arterial TEVG evidenced spontaneous pulsation consistent with motion of the native mouse artery. No significant dilation or narrowing was observed in either group during the initial 12-week period, and TEVGs were characterized by luminal matching with the adjacent host vessel without aneurysm formation or stenosis (Figure 3 A). Two animals from each group were maintained for long term evaluation up to 24 weeks, corresponding to loss of mechanical integrity based on our *in vitro* scaffold degradation studies. Mice with venous TEVGs remained healthy to 24 weeks, and explants showed viable neovessel formation after considerable scaffold degradation. However, animals from the arterial TEVG group expired at 14 weeks secondary to aneurysm and catastrophic graft rupture (Figure 3 B).

3.4 Histology and immunohistochemistry

H&E staining of arterial TEVGs at 6 and 12 weeks revealed cellular infiltration (Figure 4 A–B), but neither cell density/organization nor morphology approached that observed in the native artery (Figure 4 C). Similarly, venous TEVGs demonstrated increasing cellular infiltration over the course of 24 weeks (Figure 4 D–F) and the organization and morphology of the luminal cell layer at 24 weeks resembled that of native IVC (Figure 4 G). Masson's Trichrome staining confirmed cellular infiltration of implanted TEVGs in both groups, evidenced by integration of the adventitial layer with surrounding basal tissue, with positive staining for collagen (blue) by 12 weeks in both groups indicating the deposition of extracellular matrix (ECM) (Figure 5 A–E). Both arterial and venous TEVGs endothelialized by **6** weeks as evidenced by positive immunohistochemical staining for endothelial cells (vWF) (Figure 5 F, H). F4/80 staining was used to confirm macrophage presence and assess the degree of infiltration, and positive staining was observed through 12 weeks in both groups (Figure 5 K–N). Consistent with previous data, macrophage residence within the venous TEVG appeared to decrease by 24 weeks [59], (Figure 5 O) Staining for MMP-2 demonstrated slightly increased ECM turnover within the arterial graft wall at 6 weeks compared to 12 weeks (Figure 5 P–Q). In the venous grafts, MMP-2 expression was greatest at 6 weeks and gradually decreased at 12 and 24 weeks (Figure 5 R–T). Evidence of smooth muscle cell proliferation and integration into the neovessels was not observed; staining for α-SMA in both groups was negative (micrographs not shown).

3.5 Predictive modeling

The G&R simulations predicted a 30% dilatation in the IAA TEVG after 14 weeks of implantation, which coincides with the rapid decrease in PCLA modulus and is consistent with the time of experimentally observed rupture and increase in luminal diameter observed with ultrasound (Figure 6 B, Figure 3 A–B). The model does not currently include rupture mechanics. There was, in contrast, little predicted change in the IVC TEVG with only a 5% decrease in diameter occurring after PCLA degradation (Figure 6 A). This likely results from the accumulation of ECM that is pre-stretched, as assumed by the G&R model. This decrease in diameter is also qualitatively similar to that observed in the ultrasound measurements (Figure 3 A). As these G&R simulations were informed by grafts implanted in the IVC, the material properties for the collagenous matrix were an order of magnitude lower than those which have been previously observed for arteries in their homeostatic state (cf. Table 1 in [56]).

4. Discussion

A focused review of publications featuring *in vivo* evaluation of electrospun TEVGs highlights a critical remaining need in the field: demonstrating viability of an electrospun scaffold transforming from polymer construct to polymer-free living neovessel *in vivo* [25] (Table 1). Our current study was designed to fabricate a model electrospun TEVG, characterize graft properties and degradation rate, and evaluate the scaffold beyond degradation following implantation in a murine model. We then utilized G&R simulations to successfully predict for the first time the evolving diameter of electrospun scaffolds implanted in both the IVC and IAA based on previously fit G&R parameters. Our results highlight the utility of pairing *in silico* modeling with *in vivo* experimentation, and our hope is that the present study will provide practical feedback to improve the rational design process.

Despite many promising *in vivo* studies of electrospun TEVGs, none have reported neovessel formation beyond the point of complete polymer degradation and absorption [24,60–65]. A representative case study is presented by Walpoth and Moeller, who investigated an electrospun PCL scaffold for *in vivo* evaluation in a rat aortic interposition model for durations of 12, 24 and 78 weeks [24,62,63]. The PCL constructs lost 20% of the initial 80kDa molecular weight at 3 months, 51.5% at 12 months, and 78.1% at 18 months. It is not known, however, whether the vessel would remain mechanically stable upon 100% graft degradation because the slow degradation kinetics of PCL cannot be fully assessed in a rodent model with a lifespan of only 2 years. Our group recently showed that neovessel remodeling to a mechano-biologic steady state continues well beyond total polymer degradation [47,59,66,67]. Another recent study featured a novel scaffold composed of salt-leached poly(glycerol sebacic acid) which fully absorbed in less than three months resulting in a viable neovessel, yet residual PCL persisted at 90 days [68]. These findings at late time points illustrate the importance of long-term *in vivo* experimentation before clinical or even preclinical investigation.

With these considerations in mind, our initial design criteria required a TEVG scaffold whose degradation would occur during the lifespan of the C.B-17 SCID/bg mouse. We selected a 50:50 co-polymer of poly (ι-lactic acid) and poly (ε-caprolactone) due to the underlying mechanical properties of both strength and distensibility in combination with successful usage of this polymer in our clinical trial to treat congenital heart defects. *In vitro* we confirmed a complete loss of tensile strength by 3 months [69] (Figure 2). From a review of the relevant literature, it appears that grafts composed of randomly-oriented electrospun fibers measuring less than 1 μm in diameter inhibit transmural cellular infiltration that, in our experience, is a critical step towards forming a viable neovessel [12,25,70,71]. During electropsinning, random deposition of overlapping fibers creates void spaces between fibers resulting in a porous 3D structure: the smaller the fiber, the smaller the void space or pore, and the lower potential for cellular infiltration and tissue engraftment. However, nanofibers (fiber diameters < 1μm) have favorable cellular interactions due to similarity in scale to ECM components such as collagen fibrils.[72] This creates a challenge in choosing the ideal electrospun fiber diameter for tissue engineering: porosity comes at the cost of diminished cellular interaction. We hypothesized that a compromise between these two competing

considerations was a fiber diameter around 1μm; therefore, we iterated process parameters until we achieved fiber diameter of 882±226nm, corresponding to a pore distribution of 1-20μm (Figure 1). Since the tensile properties of the scaffold upon implantation could withstand systemic mouse arterial and venous pressures (Figure 3), we implanted the conduit in both circulations to contrast the process of neotissue formation and scaffold degradation in different hemodynamic environments.

Preliminary results were promising: implanted TEVGs in both the arterial and venous circulations demonstrated 100% patency, cellular infiltration (Figure 4), and active G&R processes (Figure 5), and they were well-integrated with adjacent native vessel as demonstrated by a high degree of luminal matching on ultrasound (Figure 3 A). Grafts were free of stenosis, thrombosis, or aneurysm formation up to 12 weeks post-implantation, which corresponds to the duration required for complete loss of graft mechanical integrity *in vitro* (Figure 1 G). Venous TEVGs remained intact up to 24 weeks and explanted specimens demonstrated a viable endothelial cell monolayer, macrophage infiltration, and ECM deposition indicative of previously reported TEVGs from our group [52,71,73,74]. Longitudinal ultrasonic analysis demonstrated that the implanted constructs integrated with native vessel over time, transitioning from a purely tubular polymeric scaffold to a living conduit with a more tortuous, vessel-like appearance. We believe this is the first report of a patent electrospun TEVG at or beyond polymer degradation *in vivo.* The animals intended for long-term follow up from the arterial implantation group experienced catastrophic graft rupture at 14 weeks, however (Figure 3 B). Critically, the TEVG failures occurred two weeks beyond the total loss of scaffold mechanical integrity as measured *in vitro*, which suggests that either neotissue formation stabilized the construct or the *in vivo* degradation rate was slower, or possibly both. The presence of organized luminal tissue, transmural cellular infiltration, and ECM deposition in both groups by week 12 suggests that the scaffold porosity permitted cellular infiltration, but overall cellularity was underwhelming (Figure 4 B, E, Figure 5 B, D, L, N, Q, S). Matrix metalloproteinase-2 was greatest at 6 weeks, indicating an active and ongoing extracellular matrix remodeling process which confirms previous reports from our group that found a peak in MMP-2 production and expression by 6 weeks that gradually decreased by 24 weeks [59,66,67] (Figure 5 P–T). However, smooth muscle cell migration and proliferation were particularly limited; our TEVG lacked formation of a robust medial layer as compared to native vessels. The small diameter electrospun PCLA scaffold presented in the current study, when implanted as an IVC interposition graft in the mouse model, demonstrated encouraging long-term results in terms of patency, engraftment, and neotissue formation.

We suggest that the catastrophic failure seen in our electrospun arterial TEVG at 14 weeks resulted from inadequate vascular neotissue formation due to three primary factors. First, electrospun nanofibers generated a relatively dense scaffold. While this did not preclude cellular infiltration, it limited the available space for macrophage infiltration and/or robust extracellular matrix deposition and subsequent remodeling. We have previously demonstrated that the degree of macrophage infiltration into the scaffold has significant impact on vascular neotissue formation, including smooth muscle cell invasion and media formation [12]. Additionally, our group has compared small-pore electrospun scaffolds to larger-pore scaffolds created by a freeze-drying process and found an improved regenerative

response using the larger-pore scaffold [47]. Taken together, these results suggest that unmodified electrospun nanofiber-scaffolds have a limited capacity for neotissue formation *in vivo*. Second, the relatively stiff nature of the scaffold under physiological loadings attenuated the mechanical stimuli experienced by the vascular neotissue (a phenomenon known as stress shielding), thereby attenuating ECM production. SMC recruitment, and subsequent remodeling. Third, polymer loss of tensile strength preceded mass loss, resulting in a non-supportive polymer structure that yet inhibited space for ECM deposition. In the absence of scaffold tensile strength, the nascent neoartery alone was unable to withstand sustained arterial pressure and likely led to the sudden rupture. This phenomenon highlights a distinction between mechanical and chemical factors, and it is critical to account for the kinetics of both processes when assessing and characterizing scaffold polymer degradation for elucidating the mechano- and immuno-mediated mechanisms of neovessel G&R.

While our current G&R simulations were not designed to predict rupture (i.e., we did not include a material damage model), the predicted rapid dilatation at long times corresponded well with experimentally observed failure and illustrates again the utility of a computational G&R model for understanding and predicting graft outcomes. Furthermore, we can change the scaffold parameter values in the model to understand their effect on the simulated time course and guide understanding of TEVG design. Modifying the scaffold modulus E_B^p to half of its original value (100 MPa) and double its original value (400 MPa) in the G&R model did little to alter the kinetics of the predicted dilatation (Supplemental Figure 1), suggesting that large changes in modulus can have limited effects on G&R when the values are orders of magnitude larger than that of the native artery [75]. Additionally, shifting the onset of rapid degradation either earlier or later did little to alter the amount of dilatation (Supplemental Figure 2). In the case where degradation did not occur in the simulated time course (solid black line, Supplemental Figure 2), no change in geometry occurred, highlighting again the need to follow experiments through to complete loss of mechanical integrity. As a proof of concept for improving outcomes, we performed alternate simulations with increased collagen material property values, and there was limited predicted dilation in the IAA TEVG (data not shown). These findings suggest that if the initial material produced by infiltrating cells had properties that approached or matched those of the native arterial ECM, it is less likely that the graft would have ruptured, as the model predicted minimal luminal changes for this case. The lack of mechanical loading of the extracellular matrix in the presence of the stiff scaffolding material could have contributed to their diminished ability to bear the arterial load. Future work will thus be aimed at utilizing our model to iteratively simulate combinations of scaffold parameters to identify those which could yield collagen with more “arterial-like” material properties, with the goal of rationally designing a small diameter arterial TEVG that resists dilation after polymer degradation and absorption. Coupling these experiments with serial bi-axial mechanical testing of the evolving neo-arteries and adjacent vessels or assessing the molecular weight loss of the remaining polymer would provide valuable insight to the fidelity of the model. Similarly, by utilizing recent advances in our computational approach, implantations in C57BL/6 Wild Type mice could inform the rational design of scaffolds for use in an immune-competent host [27].

Previous experiments demonstrated that chronic mechanical conditioning of cellular constructs in bioreactors improves mechanical behavior [76]. Similarly, slow transfer of load to the arterial neotissue could allow improved cross-linking and organization of collagenous material, such that it attains material properties similar to those of the native vessel. This highlights the importance of preventing stress shielding in developing tissues. Indeed, parametric studies extending the onset of degradation did little to alter graft outcome (Supplemental Figure 2) with dilatation occurring as polymer integrity was rapidly lost in the absence of compensatory matrix stiffening. Therefore, without following an implantation study through to complete loss of polymer mechanical integrity, it becomes difficult to conclude that the implanted design will not eventually rupture. Furthermore, gradual loading has been predicted to improve G&R outcomes for vein grafts as well, with incremental pressurization over 8 days yielding ideal mechanical adaptation [77]. This limitation underscores the critical importance of cross-talk between computational simulations and *in vivo* performance data. Ultimately, each approach can help to inform the other, permitting rapid and readily available predictions for various combinations of scaffold parameters, identifying promising iterations for *in vivo* trials.

5. Conclusions

We addressed a pressing challenge to progress in the field of small diameter tissue engineered vascular grafts, namely, the lack of a successful biodegradeable electrospun scaffold yielding a viable neovessel after complete polymer degradation *in vivo*. We used an improved rapidly degrading PCLA scaffold and demonstrated promising venous neotissue formation *in vivo*. In contrast, the same graft implanted in the arterial circulation succumbed to sudden catastrophic rupture after a loss of scaffold integrity. These results were consistent with predictions by a computational model of tissue engineered vascular graft G&R. Taken together, our data support a paradigm wherein computational modeling should inform the rational selection of scaffold parameters to fabricate TEVGs that must be followed *in vivo* for time courses extending beyond complete polymer degradation, which ultimately must be verified experimentally.

Supplementary Material

Refer to Web version on PubMed Central for supplementary material.

Acknowledgments

This work was supported, in part, by NIH grants R01 HL098228 and R01 HL128602. In addition, CAB was supported by the National Institute of General Medical Sciences of the National Institutes of Health (2T32GM068412-11A1) and JMS received support through the Graduate Student Research Fellowship from the National Science Foundation (NSF DGE1122492).

Author Disclosure Statement

CKB and TS receive research funding from Gunze Ltd. and Pall Corporation. CKB and CAB are co-founders of LYST Therapeutics, LLC. None of the funding for the work reported in this manuscript was provided by Gunze Ltd., Pall Corporation, or LYST Therapeutics, LLC.

Abbreviations:

TEVG	tissue engineered vascular graft
G&R	growth and remodeling
ECM	extracellular matrix
PCL	poly-ε-caprolactone
PCLA	poly-ε-caprolactone-co-lactic acid
P(LLA-CL)	poly (L-lactide-co-ε-caprolactone)
PGS	poly (glycerol sebacic acid)
PU	polyurethane
SEM	scanning electron microscope
SCID/bg	severe combined immunodeficient-beige
vWF	von Willebrand Factor
α-SMA	alpha smooth muscle actin
MMP-2	matrix metalloproteinase-2
EC	endothelial cell
SMC	smooth muscle cell
BM-MSC	bone marrow mesenchymal stem cell
EPC	endothelial progenitor cell
CCA	common carotid artery
IAA	infrarenal abdominal aorta
IVC	inferior vena cava
FA	femoral artery

References

[1]. Kurobe H, Maxfield MW, Breuer CK, Shinoka T, Concise review: tissue-engineered vascular grafts for cardiac surgery: past, present, and future, Stem Cells Transl Med 1 (2012) 566–571. doi:10.5966/sctm.2012-0044. [PubMed: 23197861]

[2]. Kakisis JD, Liapis CD, Breuer C, Sumpio BE, Artificial blood vessel: The Holy Grail of peripheral vascular surgery, Journal of Vascular Surgery. 41 (2005) 349–354. doi:10.1016/j.jvs.2004.12.026. [PubMed: 15768021]

[3]. Klinkert P, Post PN, of P.B.E.J., 2004, Saphenous vein versus PTFE for above-knee femoropopliteal bypass A review of the literature, Elsevier (n.d.). doi:10.1016/j.ejvs.2003.12.027.

[4]. Tara S, Rocco KA, Hibino N, Sugiura T, Kurobe H, Breuer CK, Shinoka T, Vessel bioengineering, Circ. J 78 (2014) 12–19. doi:10.1253/circj.CJ-13-1440. [PubMed: 24334558]

[5]. Teebken OE, Haverich A, Tissue engineering of small diameter vascular grafts, Eur J Vasc Endovasc Surg 23 (2002) 475–485. [PubMed: 12093061]

[6]. Udelsman BV, Maxfield MW, Breuer CK, Tissue engineering of blood vessels in cardiovascular disease: moving towards clinical translation, Heart. 99 (2013) 454–460. doi:10.1136/heartjnl-2012-302984. [PubMed: 23363931]

[7]. Cleary MA, Geiger E, Grady C, Best C, Naito Y, Breuer C, Vascular tissue engineering: the next generation, Trends in Molecular Medicine. 18 (2012) 395–405. doi:10.1016/j.molmed.2012.04.013.

[8]. Hibino N, McGillicuddy E, Matsumura G, Ishihara Y, Naito Y, Breuer C, Shinoka T, Late-term results of tissue-engineered vascular grafts in humans, The Journal of Thoracic and Cardiovascular Surgery. 139 (2010) 431–436.e2. doi:10.1016/j.jtcvs.2009.09.057. [PubMed: 20106404]

[9]. Dean EW, Udelsman B, Breuer CK, Current advances in the translation of vascular tissue engineering to the treatment of pediatric congenital heart disease, Yale J Biol Med 85 (2012) 229–238. [PubMed: 22737051]

[10]. Niklason LE, Gao J, Abbott WM, Hirschi KK, Houser S, Marini R, Langer R, Functional arteries grown in vitro, Science. 284 (1999) 489–493. [PubMed: 10205057]

[11]. L'Heureux N, Pâquet S, Labbé R, Germain L, Auger FA, A completely biological tissue-engineered human blood vessel, The FASEB Journal. 12 (1998) 47–56. [PubMed: 9438410]

[12]. Roh JD, Sawh-Martinez R, Brennan MP, Jay SM, Devine L, Rao DA, Yi T, Mirensky TL, Nalbandian A, Udelsman B, Hibino N, Shinoka T, Saltzman WM, Snyder E, Kyriakides TR, Pober JS, Breuer CK, Tissue-engineered vascular grafts transform into mature blood vessels via an inflammation-mediated process of vascular remodeling, Proc Natl Acad Sci USA. 107 (2010) 4669–4674. doi:10.1073/pnas.0911465107. [PubMed: 20207947]

[13]. Matsumura G, Isayama N, Matsuda S, Taki K, Sakamoto Y, Ikada Y, Yamazaki K, Long-term results of cell-free biodegradable scaffolds for in situ tissue engineering of pulmonary artery in a canine model, Biomaterials. 34 (2013) 6422–6428. doi:10.1016/j.biomaterials.2013.05.037. [PubMed: 23746857]

[14]. Hibino N, Duncan DR, Nalbandian A, Yi T, Qyang Y, Shinoka T, Breuer CK, Evaluation of the use of an induced puripotent stem cell sheet for the construction of tissue-engineered vascular grafts, The Journal of Thoracic and Cardiovascular Surgery. 143 (2012) 696–703. doi:10.1016/j.jtcvs.2011.06.046. [PubMed: 22244569]

[15]. Huang Z-M, Zhang YZ, Kotaki M, Ramakrishna S, A review on polymer nanofibers by electrospinning and their applications in nanocomposites, Composites Science and Technology. 63 (2003) 2223–2253. doi:10.1016/S0266-3538(03)00178-7.

[16]. Li D, Xia Y, Electrospinning of nanofibers: reinventing the wheel? Adv. Mater 16 (2004) 1151–1170. doi:10.1002/adma.200400719.

[17]. Reneker DH, Chun I, Nanometre diameter fibres of polymer, produced by electrospinning, Nanotechnology. 7 (1999) 216–223. doi:10.1088/0957-4484/7/3/009.

[18]. Ingavle GC, Leach JK, Advancements in electrospinning of polymeric nanofibrous scaffolds for tissue engineering, Tissue Engineering Part B: Reviews. 20 (2014) 277–293. doi:10.1089/ten.teb.2013.0276. [PubMed: 24004443]

[19]. D'Amore A, Amoroso N, Gottardi R, Hobson C, Carruthers C, Watkins S, Wagner WR, Sacks MS, From single fiber to macro-level mechanics: a structural finite-element model for elastomeric fibrous biomaterials. Journal of the Mechanical Behavior of Biomedical Materials. 39 (2014): 146–161. [PubMed: 25128869]

[20]. Badami AS, Kreke MR, Thompson MS, Riffle JS, Goldstein AS, Effect of fiber diameter on spreading, proliferation, and differentiation of osteoblastic cells on electrospun poly(lactic acid) substrates, Biomaterials. 27 (2006) 596–606. doi:10.1016/j.biomaterials.2005.05.084. [PubMed: 16023716]

[21]. Bashur CA, Dahlgren LA, Goldstein AS, Effect of fiber diameter and orientation on fibroblast morphology and proliferation on electrospun poly(D,L-lactic-co-glycolic acid) meshes, Biomaterials. 27 (2006) 5681–5688. doi:10.1016/j.biomaterials.2006.07.005. [PubMed: 16914196]

[22]. Wang Z, Cui Y, Wang J, Yang X, Wu Y, Wang K, Gao X, Li D, Zheng XL, Zhu Y, Kong D, Zhao Q, The effect of thick fibers and large pores of electrospun poly(e-caprolactone) vascular grafts on macrophage polarization and arterial regeneration, Biomaterials. 35 (2014) 5700–5710. doi: 10.1016/j.biomaterials.2014.03.078. [PubMed: 24746961]

[23]. Saino E, Focarete ML, Gualandi C, Emanuele E, Cornaglia AI, Imbriani M, Visai L, Effect of electrospun fiber diameter and alignment on macrophage activation and secretion of proinflammatory cytokines and chemokines, Biomacromolecules. 12 (2011) 1900–1911. doi: 10.1021/bm200248h. [PubMed: 21417396]

[24]. Pektok E, Nottelet B, Tille JC, Gurny R, Kalangos A, Moeller M, Walpoth BH, Degradation and healing characteristics of small-diameter poly(epsilon-caprolactone) vascular grafts in the rat systemic arterial circulation, Circulation. 118 (2008) 2563–2570. doi: 10.1161/CIRCULATIONAHA.108.795732. [PubMed: 19029464]

[25]. Rocco KA, Maxfield MW, Best CA, Dean EW, Breuer CK, In vivo applications of electrospun tissue-engineered vascular grafts: A review, Tissue Engineering Part B: Reviews. 20 (2014) 628–640. doi:10.1089/ten.TEB.2014.0123. [PubMed: 24786567]

[26]. Miller KS, Lee YU, Naito Y, Breuer CK, Humphrey JD, Computational model of the in vivo development of a tissue engineered vein from an implanted polymeric construct, Journal of Biomechanics. (2013) 1–8. doi:10.1016/j.jbiomech.2013.10.009. [PubMed: 23259938]

[27]. Szafron JM, Khosravi R, Reinhardt J, Best CA, Bersi MR, Yi T, Breuer CK, Humphrey JD, Immuno-driven and mechano-mediated neotissue formation in tissue engineered vascular grafts, Annals of Biomedical Engineering. (2018) 1–13. doi: 10.1007/s10439-018-2086-7.

[28]. Khosravi R, Miller KS, Best CA, Shih YC, Lee Y-U, Yi T, Shinoka T, Breuer CK, Humphrey JD, Biomechanical diversity despite mechanobiological stability in tissue engineered vascular grafts two years post-implantation, Tissue Engineering Part A. 21 (2015) 1529–1538. doi: 10.1089/ten.tea.2014.0524. [PubMed: 25710791]

[29]. Miller KS, Khosravi R, Breuer CK, Humphrey JD, A hypothesis-driven parametric study of effects of polymeric scaffold properties on tissue engineered neovessel formation, Acta Biomaterialia. 11 (2015) 283–294. doi:10.1016/j.actbio.2014.09.046. [PubMed: 25288519]

[30]. Mrowczynski W, Mugnai D, de Valence S, Tille J-C, Khabiri E, Cikirikcioglu M, Moeller M, Walpoth B, Porcine carotid artery replacement with biodegradable electrospun poly-ε-caprolactone vascular prosthesis, Journal of Vascular Surgery. 59 (2014) 210–219. doi: 10.1016/j.jvs.2013.03.004. [PubMed: 23707057]

[31]. Yao Y, Wang J, Cui Y, Xu R, Wang Z, Zhang J, Wang K, Li Y, Zhao Q, Kong D, Effect of sustained heparin release from PCL/chitosan hybrid small-diameter vascular grafts on anti-thrombogenic property and endothelialization, Acta Biomaterialia. 10 (2014) 2739–2749. doi: 10.1016/j.actbio.2014.02.042. [PubMed: 24602806]

[32]. Fukunishi T, Best CA, Sugiura T, Shoji T, Yi T, Udelsman B, Ohst D, Ong CS, Zhang H, Shinoka T, Breuer CK, Johnson J, Hibino N, Tissue-engineered small diameter arterial vascular grafts from cell-free nanofiber PCL/Chitosan scaffolds in a sheep model, PLoS ONE. 11 (2016) e0158555. doi:10.1371/journal.pone.0158555. [PubMed: 27467821]

[33]. Wang K, Zheng W, Pan Y, Ma S, Guan Y, Liu R, Zhu M, Zhou X, Zhang J, Zhao Q, Zhu Y, Wang L, Kong D, Three-layered PCL grafts promoted vascular regeneration in a rabbit carotid artery model, Macromol. Biosci 16 (2016) 608–618. doi: 10.1002/mabi.201500355. [PubMed: 26756321]

[34]. Chan AHP, Tan RP, Michael PL, Lee BSL, Vanags LZ, Ng MKC, Bursill CA, Wise SG, Evaluation of synthetic vascular grafts in a mouse carotid grafting model, PLoS ONE. 12 (2017) e0174773–15. doi:10.1371/journal.pone.0174773. [PubMed: 28355300]

[35]. Ju YM, Ahn H, Arenas-Herrera J, Kim C, Abolbashari M, Atala A, Yoo JJ, Lee SJ, Electrospun vascular scaffold for cellularized small diameter blood vessels: A preclinical large animal study, Acta Biomaterialia. 59 (2017) 58–67. doi:10.1016/j.actbio.2017.06.027. [PubMed: 28642016]

[36]. Pan Y, Zhou X, Wei Y, Zhang Q, Wang T, Zhu M, Li W, Huang R, Liu R, Chen J, Fan G, Wang K, Kong D, Zhao Q, Small-diameter hybrid vascular grafts composed of polycaprolactone and polydioxanone fibers, Nature Publishing Group. 7 (2017) 1333–11. doi: 10.1038/s41598-017-03851-1.

[37]. Tang Di Chen S, Hou D, Gao J, Jiang L, Shi J, Liang Q, Kong D, Wang S, Regulation of macrophage polarization and promotion of endothelialization by NO generating and PEG-YIGSR modified vascular graft, Materials Science & Engineering C. 84 (2018) 1–11. doi:10.1016/j.msec.2017.11.005. [PubMed: 29519417]

[38]. Wang K, Zhang Q, Zhao L, Pan Y, Wang T, Zhi D, Ma S, Zhang P, Zhao T, Zhang S, Li W, Zhu M, Zhang J, Qiao M, Kong D, Functional modification of electrospun poly(e-caprolactone) vascular grafts with the fusion protein VEGF–HGFI enhanced vascular regeneration, ACS Appl. Mater. Interfaces. 9 (2017) 11415–11427. doi:10.1021/acsami.6b16713. [PubMed: 28276249]

[39]. Wu Y, Qin Y, Wang Z, Wang J, Zhang C, Li C, Kong D, The regeneration of macro-porous electrospun poly(ε-caprolactone) vascular graft during long-term in situ implantation, J. Biomed. Mater. Res 106 (2017) 1618–1627. doi:10.1002/jbm.b.33967.

[40]. Gao J, Jiang L, Liang Q, Shi J, Hou D, Tang D, Chen S, Kong D, Wang S, The grafts modified by heparinization and catalytic nitric oxide generation used for vascular implantation in rats, Regenerative Biomaterials. 5 (2018) 105–114. doi:10.1093/rb/rby003. [PubMed: 29644092]

[41]. Huang R, Gao X, Wang J, Chen H, Tong C, Tan Y, Tan Z, Triple-layer vascular grafts fabricated by combined E-jet 3D printing and electrospinning, Annals of Biomedical Engineering. 46 (2018) 1254–1266. doi:10.1007/s10439-018-2065-z. [PubMed: 29845412]

[42]. Madhavan K, Elliot W, Tan Y, Monnet E, Tan W, Performance of marrow stromal cell-seeded small-caliber multilayered vascular graft in a senescent sheep model, Biomedical Materials. 13 (2018) 055004–14. doi:10.1088/1748-605X/aac7a6. [PubMed: 29794344]

[43]. Fukunishi T, Best CA, Sugiura T, Opfermann J, Ong CS, Shinoka T, Breuer CK, Krieger A, Johnson J, Hibino N, Preclinical study of patient-specific cell-free nanofiber tissue-engineered vascular grafts using 3-dimensional printing in a sheep model, The Journal of Thoracic and Cardiovascular Surgery. 153 (2017) 924–932. doi: 10.1016/j.jtcvs.2016.10.066. [PubMed: 27938900]

[44]. Hu YT, Pan XD, Zheng J, Ma WG, Sun LZ, In vitro and in vivo evaluation of a small-caliber coaxial electrospun vascular graft loaded with heparin and VEGF, Int J Surg 44 (2017) 244–249. doi:10.1016/j.ijsu.2017.06.077. [PubMed: 28648794]

[45]. Fukunishi T, Best CA, Ong CS, Groehl T, Reinhardt J, Yi T, Miyachi H, Zhang H, Shinoka T, Breuer CK, Johnson J, Hibino N, Role of bone marrow mononuclear cell seeding for nanofiber vascular grafts, Tissue Engineering Part A. 24 (2018) 135–144. doi:10.1089/ten.TEA.2017.0044. [PubMed: 28486019]

[46]. Henry JJD, Yu J, Wang A, Lee R, Fang J, Li S, Engineering the mechanical and biological properties of nanofibrous vascular grafts for in situ vascular tissue engineering, Biofabrication. 9 (2017) 035007. doi:10.1088/1758-5090/aa834b. [PubMed: 28817384]

[47]. Tara S, Kurobe H, Rocco KA, Maxfield MW, Best CA, Yi T, Naito Y, Breuer CK, Shinoka T, Well-organized neointima of large-pore poly(l-lactic acid) vascular graft coated with poly(l-lactic-co-ε-caprolactone) prevents calcific deposition compared to small-pore electrospun poly(l-lactic acid) graft in a mouse aortic implantation model, Atherosclerosis. 237 (2014) 684–691. doi: 10.1016/j.atherosclerosis.2014.09.030. [PubMed: 25463106]

[48]. Khosravi R, Best CA, Allen RA, Stowell CET, Onwuka E, Zhuang JJ, Lee YU, Yi T, Bersi MR, Shinoka T, Humphrey JD, Wang Y, Breuer CK, Long-term functional efficacy of a novel electrospun poly(glycerol sebacate)-based arterial graft in mice, Annals of Biomedical Engineering. (2016) 1–16. doi:10.1007/s10439-015-1545-7. [PubMed: 26620776]

[49]. Bergmeister H, Seyidova N, Schreiber C, Strobl M, Grasl C, Walter I, Messner B, Baudis S, Frohlich S, Marchetti-Deschmann M, Griesser M, di Franco M, Krssak M, Liska R, Schima H, Biodegradable, thermoplastic polyurethane grafts for small diameter vascular replacements, Acta Biomaterialia. 11 (2015) 104–113. doi: 10.1016/j.actbio.2014.09.003. [PubMed: 25218664]

[50]. Guo HF, Dai WW, Qian DH, Qin ZX, Lei Y, Hou XY, Wen C, A simply prepared small-diameter artificial blood vessel that promotes in situ endothelialization, Acta Biomaterialia. 54 (2017) 107–116. doi:10.1016/j.actbio.2017.02.038. [PubMed: 28238915]

[51]. Qiu X, Lee BLP, Ning X, Murthy N, Dong N, Li S, End-point immobilization of heparin on plasma-treated surface of electrospun polycarbonate-urethane vascular graft, Acta Biomaterialia. 51 (2017) 138–147. doi: 10.1016/j.actbio.2017.01.012. [PubMed: 28069505]

[52]. Roh JD, Nelson GN, Brennan MP, Mirensky TL, Yi T, Hazlett TF, Tellides G, Sinusas AJ, Pober JS, Saltzman WM, Kyriakides TR, Breuer CK, Small-diameter biodegradable scaffolds for functional vascular tissue engineering in the mouse model, Biomaterials. 29 (2008) 1454–1463. doi: 10.1016/j.biomaterials.2007.11.041. [PubMed: 18164056]

[53]. Humphrey JD, Rajagopal KR, A constrained mixture model for growth and remodeling of soft tissues, World Scientific, (n.d.). doi:10.1142/S0218202502001714.

[54]. Garg K, Pullen NA, Oskeritzian CA, Ryan JJ, Bowlin GL, Macrophage functional polarization(M1/M2) in response to varying fiber and pore dimensions of electrospun scaffolds, Biomaterials. 34 (2013) 4439–4451. doi:10.1016/j.biomaterials.2013.02.065. [PubMed: 23515178]

[55]. Sussman EM, Halpin MC, Muster J, Moon RT, Ratner BD, Porous implants modulate healing and induce shifts in local macrophage polarization in the foreign body reaction, Annals of Biomedical Engineering. 42 (2013) 1508–1516. doi:10.1007/s10439-013-0933-0. [PubMed: 24248559]

[56]. Valentin A, Cardamone L, Baek S, Humphrey JD, Complementary vasoactivity and matrix remodelling in arterial adaptations to altered flow and pressure, J. R. Soc. Interface. 6 (2009) 293–306. doi:10.1098/rsif.2008.0254. [PubMed: 18647735]

[57]. Humphrey JD, Vascular adaptation and mechanical homeostasis at tissue, cellular, and sub-cellular levels, Cell Biochem. Biophys 50 (2008) 53–78. doi:10.1007/s12013-007-9002-3. [PubMed: 18209957]

[58]. Cohn D, Hotovely Salomon A, Designing biodegradable multiblock PCL/PLA thermoplastic elastomers, Biomaterials. 26 (2005) 2297–2305. doi: 10.1016/j.biomaterials.2004.07.052. [PubMed: 15585232]

[59]. Naito Y, Williams-Fritze M, Duncan DR, Church SN, Hibino N, Madri JA, Humphrey JD, Shinoka T, Breuer CK, Characterization of the Natural History of Extracellular Matrix Production in Tissue-Engineered Vascular Grafts during Neovessel Formation, Cells Tissues Organs. 195 (2012) 60–72. doi:10.1159/000331405. [PubMed: 21996715]

[60]. Hashi CK, Derugin N, Janairo RRR, Lee R, Schultz D, Lotz J, Li S, Antithrombogenic Modification of Small-Diameter Microfibrous Vascular Grafts, Arteriosclerosis, Thrombosis, and Vascular Biology. 30 (2010) 1621–1627. doi:10.1161/ATVBAHA.110.208348.

[61]. Hashi CK, Zhu Y, Yang GY, Young WL, Hsiao BS, Wang K, Chu B, Li S, Antithrombogenic property of bone marrow mesenchymal stem cells in nanofibrous vascular grafts, Proc Natl Acad Sci USA. 104 (2007) 11915–11920. doi:10.1073/pnas.0704581104. [PubMed: 17615237]

[62]. de Valence S, Tille JC, Mugnai D, Mrowczynski W, Gurny R, Moller M, Walpoth BH, Long term performance of polycaprolactone vascular grafts in a rat abdominal aorta replacement model, Biomaterials. 33 (2012) 38–47. doi:10.1016/j.biomaterials.2011.09.024. [PubMed: 21940044]

[63]. Nottelet B, Pektok E, Mandracchia D, Tille JC, Walpoth B, Gurny R, Moller M, Factorial design optimization and in vivo feasibility of poly(ε-caprolactone)-micro- and nanofiber-based small diameter vascular grafts, Wiley Online Library, (n.d.). doi:10.1002/jbm.a.32023.

[64]. Wise SG, Byrom MJ, Waterhouse A, Bannon PG, Ng MKC, Weiss AS, A multilayered synthetic human elastin/polycaprolactone hybrid vascular graft with tailored mechanical properties, Acta Biomaterialia. 7 (2011) 295–303. doi:10.1016/j.actbio.2010.07.022. [PubMed: 20656079]

[65]. Tillman BW, Yazdani SK, Lee SJ, Geary RL, Atala A, Yoo JJ, The in vivo stability of electrospun polycaprolactone-collagen scaffolds in vascular reconstruction, Biomaterials. 30 (2009) 583–588. doi: 10.1016/j.biomaterials.2008.10.006. [PubMed: 18990437]

[66]. Naito Y, Lee YU, Yi T, Church SN, Solomon D, Humphrey JD, Shinoka T, Breuer CK, Beyond burst pressure: Initial evaluation of the natural history of the biaxial mechanical properties of tissue-engineered vascular grafts in the venous circulation using a murine model, Tissue Engineering Part A. 20 (2014) 346–355. doi:10.1089/ten.tea.2012.0613. [PubMed: 23957852]

[67]. Udelsman BV, Khosravi R, Miller KS, Dean EW, Bersi MR, Rocco K, Yi T, Humphrey JD, Breuer CK, Characterization of evolving biomechanical properties of tissue engineered vascular grafts in the arterial circulation, Journal of Biomechanics. 47 (2014) 2070–2079. doi:10.1016/j.jbiomech.2014.03.011. [PubMed: 24702863]

[68]. Wu W, Allen RA, Wang Y, Fast-degrading elastomer enables rapid remodeling of a cell-free synthetic graft into a neoartery, Nature Medicine. 18 (2012) 1148–1153. doi:10.1038/nm.2821.

[69]. Patterson JT, Gilliland T, Maxfield MW, Church S, Naito Y, Shinoka T, Breuer CK, Tissue-engineered vascular grafts for use in the treatment of congenital heart disease: From the bench to the clinic and back again, Regenerative Medicine. 7(2012), 409–419. doi:10.2217/rme.12.12 [PubMed: 22594331]

[70]. Tara S, Kurobe H, Rocco KA, Maxfield MW, Best CA, Yi T, Naito Y, Breuer CK, Shinoka T, Well-organized neointima of large-pore poly(l-lactic acid) vascular graft coated with poly(l-lactic-co-ε-caprolactone) prevents calcific deposition compared to small-pore electrospun poly(l-lactic acid) graft in a mouse aortic implantation model, Atherosclerosis. 237 (2014) 684–691. doi: 10.1016/j.atherosclerosis.2014.09.030. [PubMed: 25463106]

[71]. Hibino N, Yi T, Duncan DR, Rathore A, Dean E, Naito Y, Dardik A, Kyriakides T, Madri J, Pober JS, Shinoka T, Breuer CK, A critical role for macrophages in neovessel formation and the development of stenosis in tissue-engineered vascular grafts, The FASEB Journal. 25 (2011) 4253–4263. doi:10.1096/fj.11-186585. [PubMed: 21865316]

[72]. Li WJ, Laurencin CT, Caterson EJ, Tuan RS, Ko FK, Electrospun nanofibrous structure: a novel scaffold for tissue engineering, J. Biomed. Mater. Res 60 (2002) 613–621. [PubMed: 11948520]

[73]. Hibino N, Villalona G, Pietris N, Duncan DR, Schoffner A, Roh JD, Yi T, Dobrucki LW, Mejias D, Sawh-Martinez R, Harrington JK, Sinusas A, Krause DS, Kyriakides T, Saltzman WM, Pober JS, Shin'oka T, Breuer CK, Tissue-engineered vascular grafts form neovessels that arise from regeneration of the adjacent blood vessel, The FASEB Journal. 25 (2011) 2731–2739. doi: 10.1096/fj.11-182246. [PubMed: 21566209]

[74]. Tara S, Kurobe H, Maxfield MW, Rocco KA, Yi T, Naito Y, Breuer CK, Shinoka T, Evaluation of remodeling process in small-diameter cell-free tissue-engineered arterial graft, Journal of Vascular Surgery. 62 (2015) 734–743. doi:10.1016/j.jvs.2014.03.011. [PubMed: 24745941]

[75]. Ferruzzi J, Bersi MR, Uman S, Yanagisawa H, Humphrey JD, Decreased elastic energy storage, not increased material stiffness, characterizes central artery dysfunction in fibulin-5 deficiency independent of sex, Journal of Biomechanical Engineering. 137, no. 3 (2015): 0310007.

[76]. Huang AH, Balestrini JL, Udelsman BV, Zhou KC, Zhao L, Ferruzzi J, Starcher BC, Levene MJ, Humphrey JD, Niklason LE, Biaxial stretch improves elastic fiber maturation, collagen arrangement, and mechanical properties in engineered arteries, Tissue Engineering Part C: Methods. 22 (2016) 524–533. doi:10.1089/ten.tec.2015.0309.

[77]. Ramachandra AB, Humphrey JD, Marsden AL, Gradual loading ameliorates maladaptation in computational simulations of vein graft growth and remodelling, J. R. Soc. Interface. 14 (2017) 20160995–12. doi:10.1098/rsif.2016.0995. [PubMed: 28566510]

Statement of Significance

Herein, we apply a biodegradable electrospun vascular graft to the arterial and venous circulations of the mouse and follow recipients beyond the point of polymer degradation. While venous implants formed viable neovessels, arterial grafts experienced catastrophic rupture due to aneurysmal dilation. We then inform a previously developed computational model of tissue engineered vascular graft growth and remodeling with parameters specific to the electrospun scaffolds utilized in this study. Remarkably, model simulations predict the differential performance of the venous and arterial constructs over 24 weeks. We conclude that computational simulations should inform the rational selection of scaffold parameters to fabricate tissue engineered vascular grafts that must be followed *in vivo* over time courses extending beyond polymer degradation.

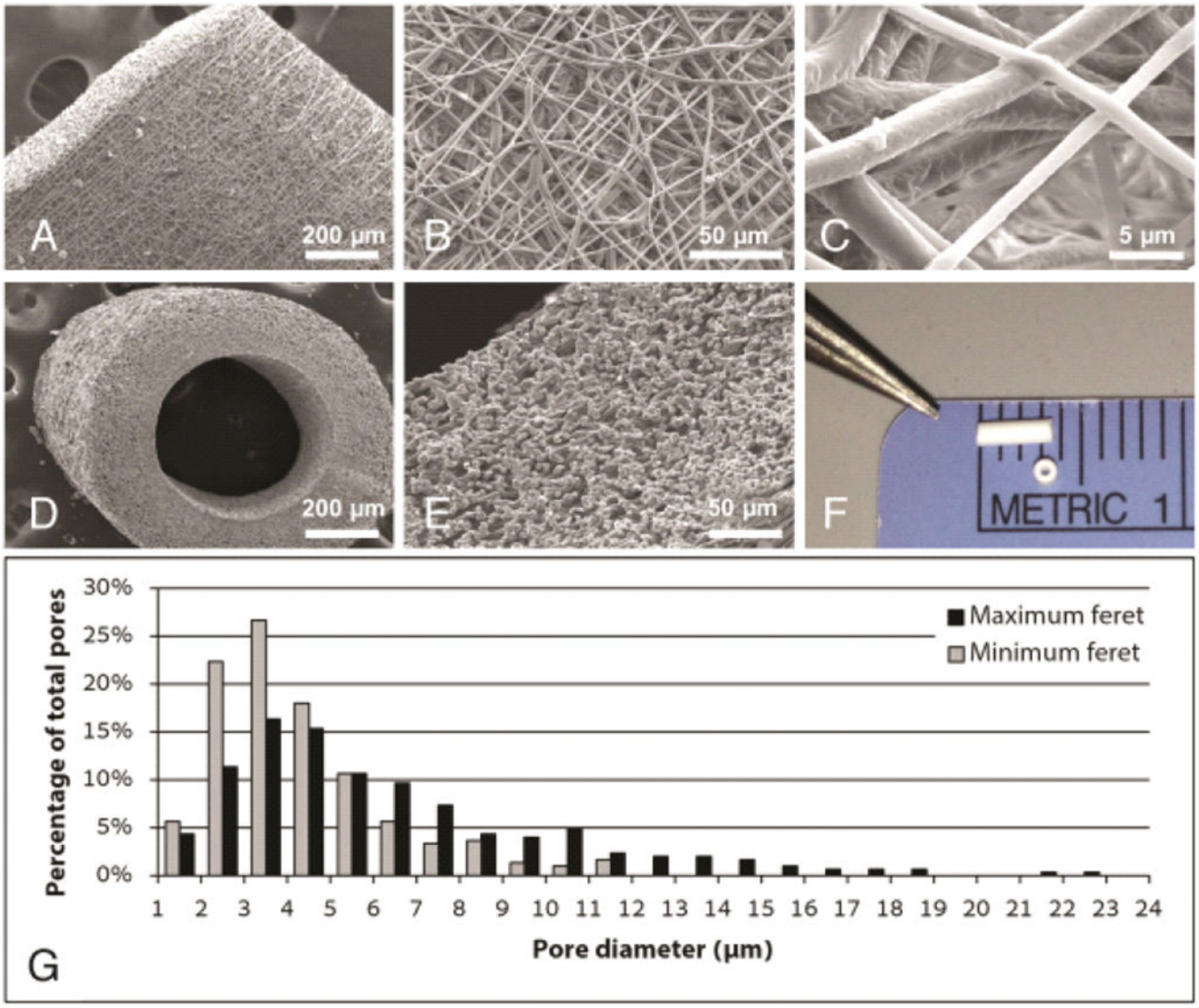

Fig. 1.

Electrospun scaffold characterization. Scanning electron microscope (SEM) imaging of the graft wall at (A) 100×, (B) 500×, and (C) 4000× demonstrating the microstructural characteristics of the electrospun scaffold. Sub-1 μm diameter polymeric fibers (average 882 ± 226 nm) overlap to form a porous tubular conduit. SEM images of the scaffold in cross-section at (D) 100× and (E) 400× highlight the wall thickness (average 234.8 ± 20.3 μm), three-dimensional porosity, and luminal diameter (average 526.4 ± 22.6 μm) of the graft. A gross image (F) of the TEVG prior to implantation demonstrates the scale of the murine graft. (G) Pore size distribution based on measurements of maximum and minimum Feret diameters.

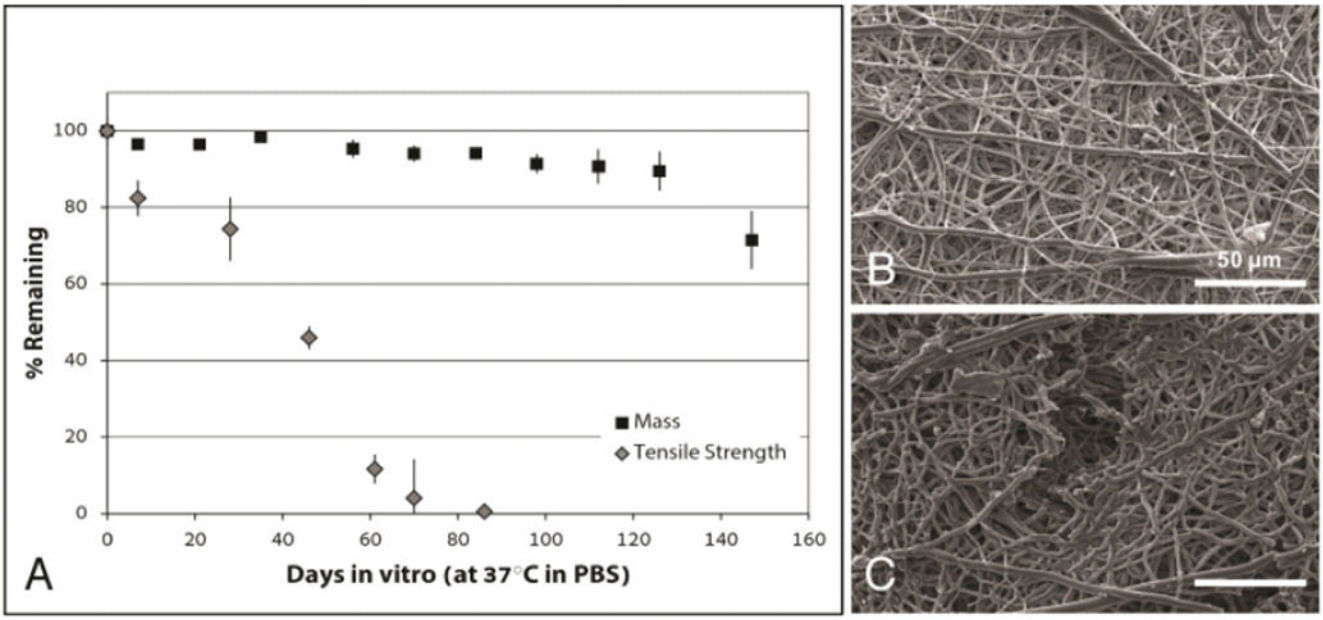

Fig. 2.

In vitro degradation of electrospun PCLA grafts. Grafts were incubated in PBS at 37 °C and longitudinally assessed for mass and uniaxial tensile strength. (A) Graph of resulting data (mean ± SEM) reported as percentages of original values as measured at day 0. Grafts lost approximately 50% of original tensile strength by 7 weeks and exhibited complete loss of tensile strength by week 12. In comparison, graft mass was approximately 94% of the original value at 12 weeks and decreased to approximately 70% at 21 weeks. Scanning electron images of the graft surface at (B) 12 weeks present no evidence of degradation but at (C) 18 weeks signs of fiber degradation and fissuring were apparent.

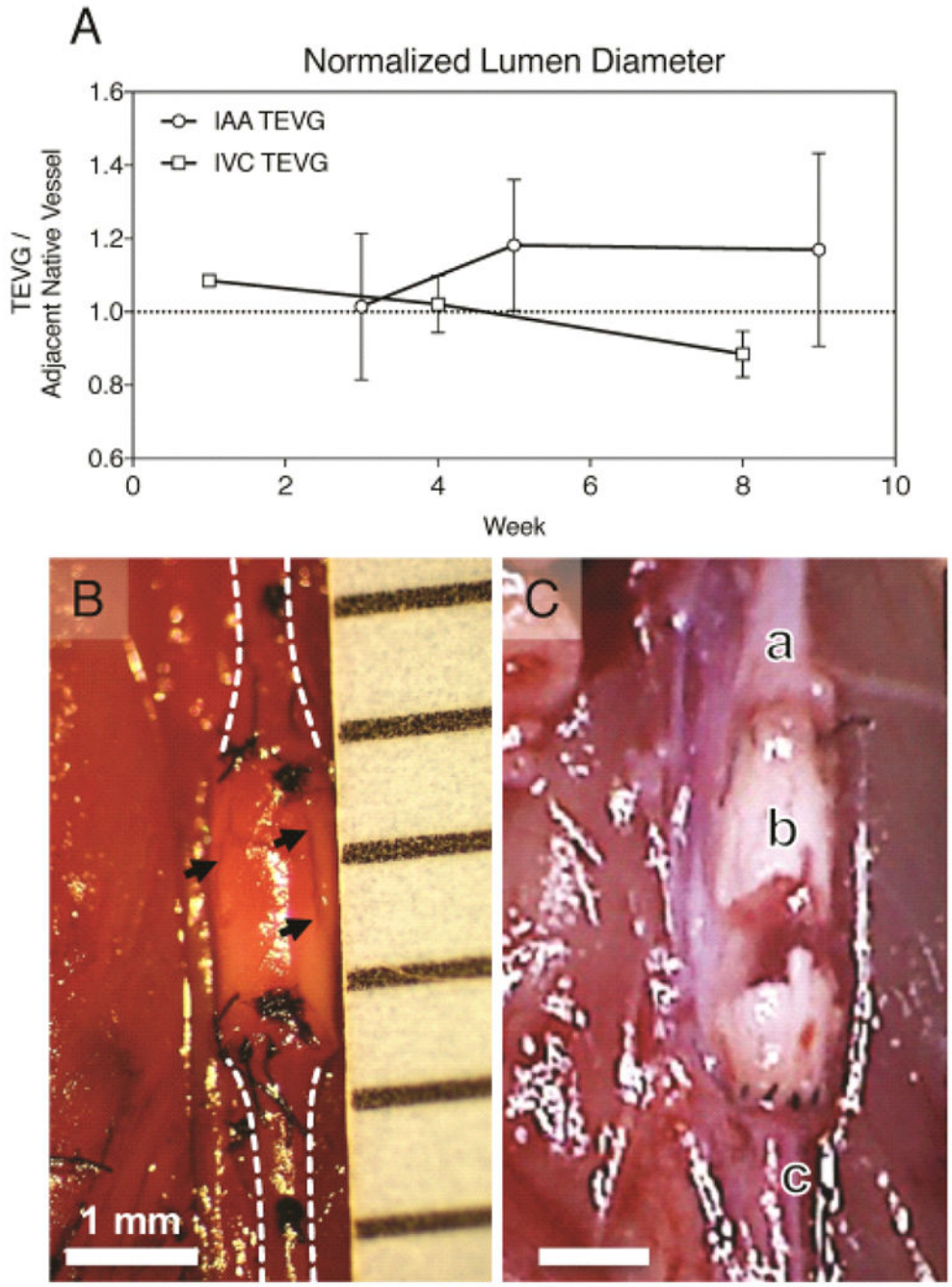

Fig. 3.

In vivo assessment of venous and arterial TEVGs. Serial ultrasound measurements of graft and adjacent native inferior vena cava or abdominal aortic segments were performed over 10 weeks. (A) Plot comparing average luminal diameters of implanted TEVGs normalized to the adjacent vessel diameter as acquired by transabdominal ultrasound. There was no significant change in luminal diameter over this period between groups. However, after 4 weeks arterial grafts demonstrated progressive dilation and venous grafts progressive narrowing. (B) In situ image of an electrospun PCLA vascular graft 6 weeks after surgical

implantation in the arterial circulation compared with a ruptured arterial TEVG 14 weeks after implantation. In both images: A) Proximal aorta. B) Electrospun PCLA graft. C) Distal aorta. Arrows indicate observed areas of electrospun TEVG degradation.

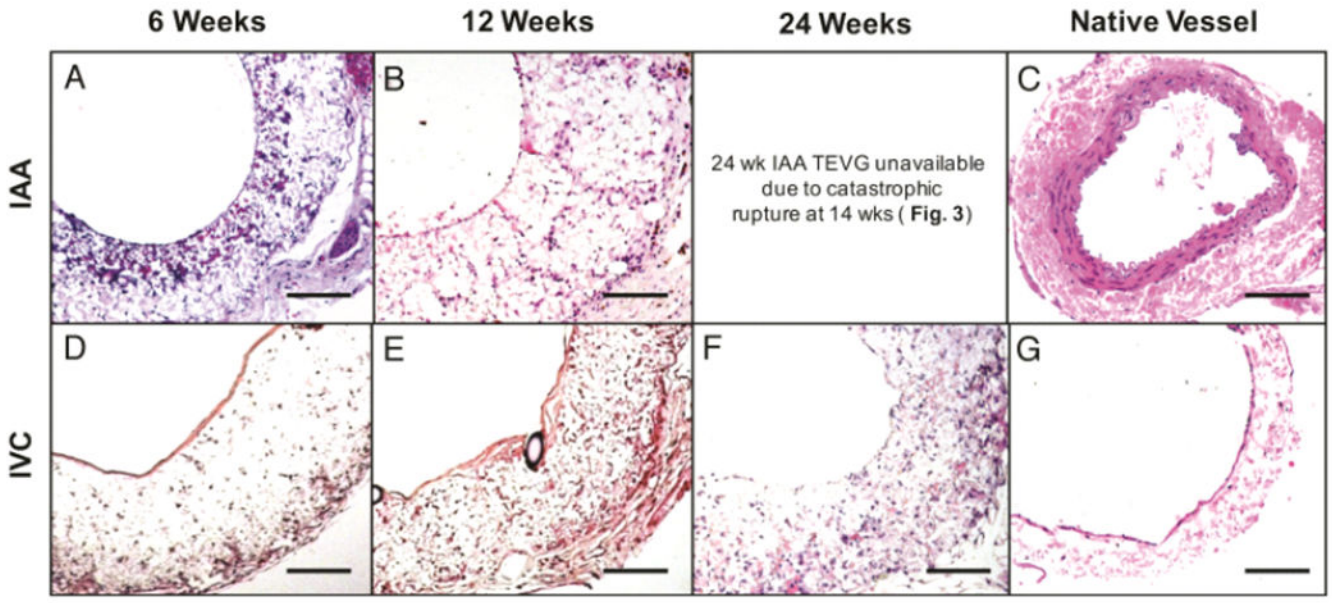

Fig. 4.

TEVG Histology. Hematoxylin and eosin (H&E) staining of explanted arterial grafts at 6 (A) and 12 (B) weeks post-implantation compared to native SCID/bg IAA (C), and venous grafts at 6 (D), 12 (E), and 24 (F) weeks post-implantation compared to the native IVC (G). All photomicrographs acquired at 20× magnification. Scale bar = 100μm.

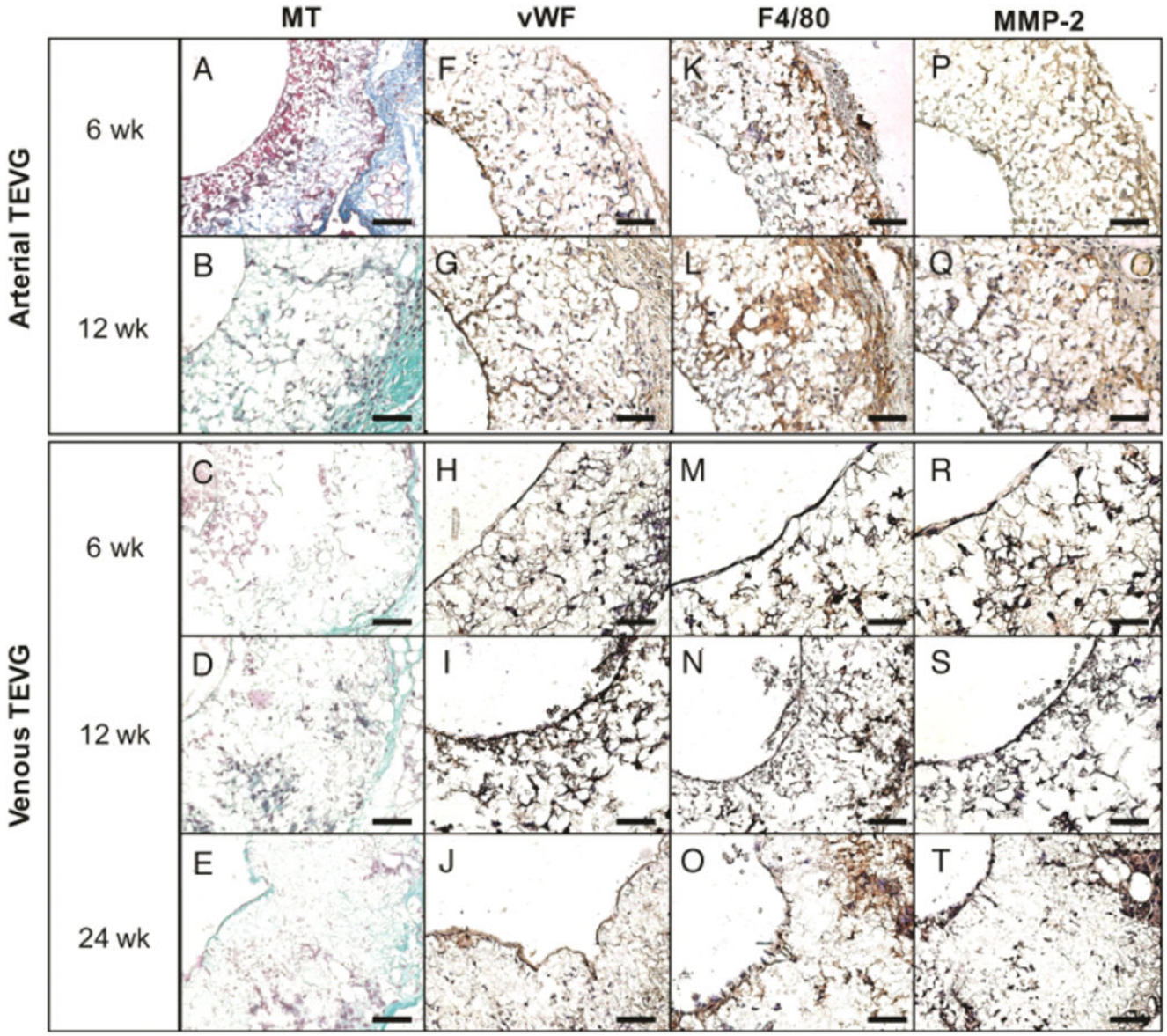

Fig. 5.

Neotissue formation and remodeling in arterial and venous TEVGs. Histologic and immunohistochemical evaluation of explanted arterial grafts at 6 (A, F, K, P) and 12 (B, G, L, Q) weeks post implantation and explanted venous grafts at 6 (C, H, M, R), 12 (D, I, N, S), and 24 (E, J, O, T) weeks post implantation. MT (A-E) identified extracellular matrix deposition, vWF (F-J) demonstrated the development of a confluent endothelial cell monolayer by 12 weeks in both groups, F4/80 (K-O) identified macrophage infiltration and proliferation and MMP-2 (P-T) evidenced ECM turnover and active tissue remodeling. All photomicrographs at 40× magnification. Scale bar = 50μm.

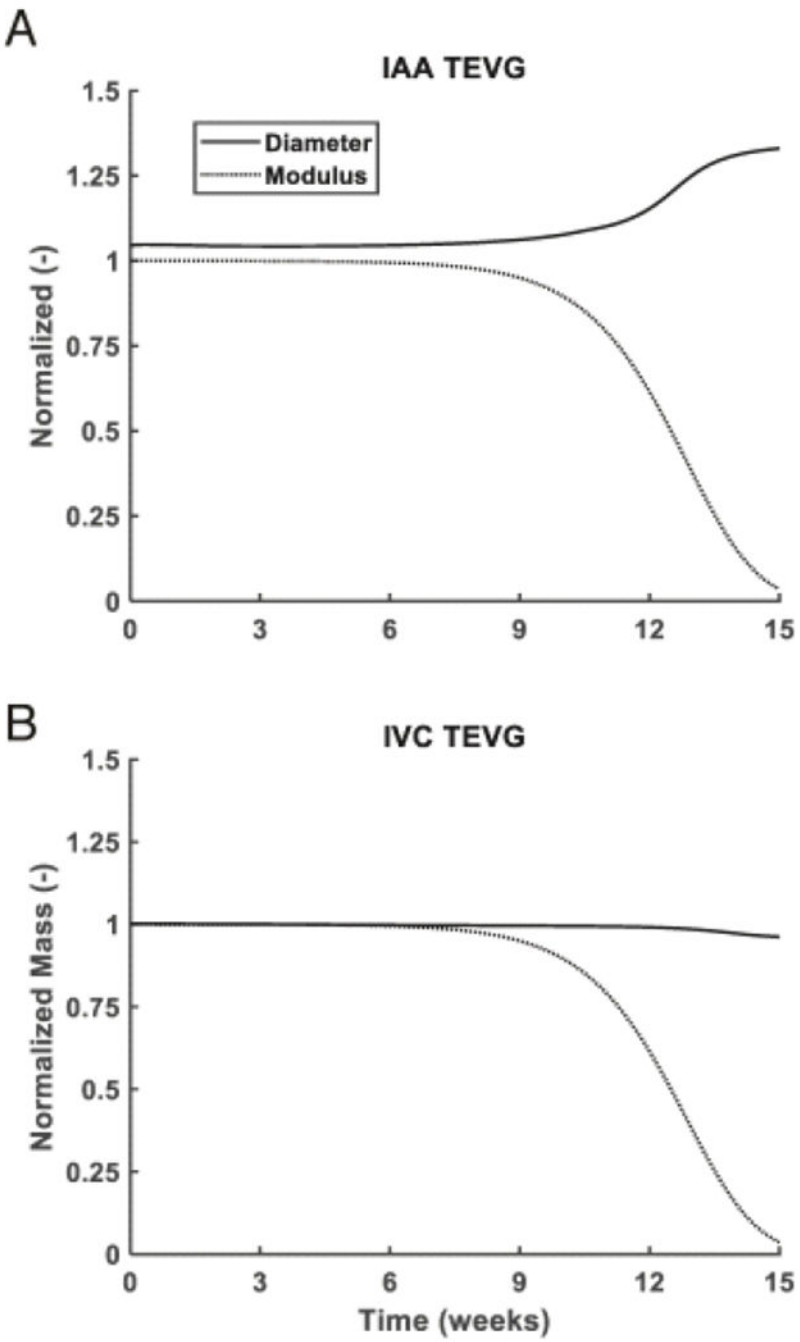

Fig. 6.

Predicting electrospun TEVG modulus and diameter over 15 weeks. Simulated evolution of normalized loaded TEVG diameter and PCLA modulus in the IAA (A) and IVC (B), as predicted by G&R. Diameters are normalized by initial unloaded graft diameter and modulus is normalized by initial modulus. Computational predictions indicated a slight narrowing of IVC TEVG diameter associated with modulus loss of the scaffold due to the pre-stretch of deposited matrix in G&R. Parameters incorporated into the model are defined in Table 2. In the artery, the TEVG was predicted to rapidly dilate concurrent with loss of

scaffold integrity. The simulated trends in diameter change are similar to those observed in vivo and validate the utility of in silico studies prior to in vivo experiments when assessing novel biodegradable vascular conduits.

Table 1.

An updated literature review (2014 to 2018) summarizing *in vivo* applications of electrospun tissue engineered vascular grafts. Although a variety of polymer types and modifications have been investigated, none have yielded a functional neovessel beyond the point of complete polymer degradation. PCL (poly caprolactone), P(LLA-CL) (poly (L-lactide-co-ε-caprolactone), PGS (poly (glycerol sebacic acid)), PU (polyurethane), Y / N (Yes / No), ECs (endothelial cells), SMCs (smooth muscle cells), BM-MSCs (bone marrow-mesenchymal stem cells), EPCs (endothelial progenitor cells), CCA (common carotid artery), IAA (infrarenal abdominal aorta), IVC (inferior vena cava), FA (femoral artery), NR (not reported), NA (not assessed).

Polymer	***TEVG Design***	***Cell Seeding***	***Graft ID (mm)***	***Grafting Model (Animal)***	***Weeks In-Vivo***	***Patency***	***Endothelium (Weeks)***	***Neo-intima***	***Cellular Infiltration***	***Fiber Diameter (μm)***	***Complete Degradation?***	***Year***	***Ref.***
PCL	ES graft as-spun	N	4.0	CCA (Pigs)	4	100%	4 (86%)	Y	Y	2.2 ± 0.6	N	2014	[30]
	Tri-layered PCL and chitosan draft	N	1.5	IAA (Rats)	4	75%	4	Y	Y	PCL - 0.591 ± 0.05			
CS - 0.305 ± 0.04	N	2014	[31]										
	PCL/Chitosan (20:1)	N	1.0	IAA (Mice)	36	100%	36	-	-	0.150 ± 0.06	N	2016	[32]
	PCL/Chitosan (20:1)	N	5.0	CCA (Sheep)	36	67%	36	Y	Y	0.150 ± 0.06	N	2016	[33]
	Tri-layered PCL graft	N	2.2	CCA (Rabbits)	12	100%	12 (83.1%)	Y	Y	Inner - 0.81 ± 0.45			
Middle - 0.85 ± 0.31													
Outer - 0.95 ± 0.44	N	2016	[34]										
	ES graft as-spun	N	0.5	CCA (Rats)	4	83%	4 (78.5%)	Y	Y	0.39 ± 0.01	N	2017	[34]
	PCL and Collagen I (1:1)	ECs,											
SMCs	4.75	CCA (Sheep)	24	100%	24	Y	Y	Inner - 4.45 ± 0.81					
Outer - 0.27 ± 0.09	N	2017	[35]										
	PCL/PDS	N	2	IAA (Rats)	12	80%	4 (83.3%)	Y	Y	NR	N	2017	[36]
	PCL w/coated layers	N	2	IAA (Rats)	8	100%	8 (75%)	Y	Y	5.66 ± 0.41	N	2017	[37]
	PCL w/modified surface	N	2	IAA (Rats)	4	100%	4 (82.7%)	Y	Y	7.06 ± 0.76	N	2017	[38]
	ES graft as-spun	N	2.0	IAA (Rats)	52	100%	52	Y	Y	6.8 ± 1.3	N	2017	[39]
	PCL w/coated layer	N	2	IAA (Rats)	8	100%	8	Y	Y	6.41 ± 1.15	N	2018	[40]
	Layers of PCL or PCL/PEG	N	2.0	IAA (Rats)	12	NR	12	Y	Y	NR	N	2018	[41]
	PCL graft coated w/collagen-chitosan	BM-MSCs	5.56	CCA (Sheep)	4	100.0%	N	Y	Y	NR	N	2018	[42]
P(LLA-CL)													
	P(LLA-CL) and PGA (1:1)	N	12	IVC (Sheep)	36	100%	36	Y	Y	NR	N *	2017	[43]
	P(LLA-CL) graft spun w/ Col I and elastin (80: 10: 10)	N	4	IAA (Rabbits)	4	93.0%	4	Y	Y	NR	N	2017	[44]

Polymer	*TEVG Design*	*Cell Seeding*	*Graft ID (mm)*	*Grafting Model (Animal)*	*Weeks In-Vivo*	*Patency*	*Endothelium (Weeks)*	*Neo-intima*	*Cellular Infiltration*	*Fiber Diameter (μm)*	*Complete Degradation?*	*Year*	*Ref.*
	P(LLA-CL) and PGA (1:1)	BM-MNCs	1	IVC (Mice)	36	90%	36	Y	Y	0.61 ± 0.27	N	2018	[45]
PLLA													
	PLLA/PCL	N	1	CCA (Rats)	4	88%	2 (82%)	Y	Y	0.7-1.0	N	2018	[46]
	ES graft as spun	N	0.5-0.6	IAA (Mice)	52	87.5%	52	Y	N	0.7	N	2015	[47]
PGS													
	PGS core w/ PCL sheath	N	0.78	IAA (Mice)	52	100%	NA	Y	Y	PGS - 1.45 ± 0.06			
PCL - NR	N	2016	[48]										
PU													
	ES graft as-spun	N	1.5	IAA (Rats)	52	100%	4	Y	Y	1.39 ± 0.76	N	2015	[49]
	PU w/protein modification	EPCs	3	FA (Dogs)	24	63%	NA	Y	Y	0.45 ± 0.14	N	2017	[50]
	PU w/modified surface	N	1	CCA (Rats)	4	86%	4	Y	Y	0.497 ± 0.316	N	2017	[51]

* 2.09±0.69% of scaffolding material remained at 6 months post-implantation.

Table 2.

Parameters characterizing G&R of the electrospun PCLA scaffolds. With the exception of PCLA modulus, all scaffold parameters were determined by data collected in this study. [a] from [56]

Parameter	Description	Value	Units
r^p	Scaffold pore size	3.34	μm
ω^p	Scaffold fiber diameter	0.88	μm
e^p	Scaffold porosity	85	%
E_B^p	PCLA Young's-type modulus[a]	200	MPa
k_E^p	PCLA degradation rate	0.075	1/days
ζ_E^p	PCLA degradation shape	150	days
γ_D^i	*In vivo* degradation modifier	1.25	-